Accepted by Cement and Concrete Composites (2007).

X-Ray Absorption Studies of Drying of Cementitious Tile Adhesive Mortars

Dale P. Bentz[a,*], Claus-Jochen Haecker[b], Max A. Peltz[a], and Kenneth A. Snyder[a]

[a] Materials and Construction Research Division
Building and Fire Research Laboratory
National Institute of Standards and Technology
Gaithersburg, MD 20899-8615
dale.bentz@nist.gov
max.peltz@nist.gov
kenneth.snyder@nist.gov
[b] SE Tylose GmbH & Co. KG (Shin-Etsu Chemical)
Rheingaustrasse 190 - 196, Building H346
65203 Wiesbaden, Germany
clausjochen.haecker@SETylose.de

Abstract

X-ray absorption measurements have been applied to studying film formation at the exposed surface during the drying of cementitious tile adhesive mortars as a function of ingredients and mixture proportions. Preliminary observations suggested that in addition to a drying front, concurrently, a densification front is observed proceeding from the exterior of the specimens inward. Due to the extremely high viscosity of the pore "solution" in these mortars, an analysis based on Stokes equation actually suggests that some of the smaller cement particles will be "carried" along with the drying pore solution to the top surface of the specimen where they are sequentially deposited. To verify this hypothesis, further experiments were conducted using either a coarse cement or a fine limestone as a total replacement for the commonly used cement. The x-ray absorption results are further supported by concurrent mass loss measurements on equivalent specimens for each experiment and by particle size distribution analysis of the final dried limestone/silica sand system as a function of depth.

Keywords: Building technology; drying; film formation; mortar; tile adhesive; viscosity; x-ray absorption.

Introduction

Specialty thin layer mortars are often formulated for usage as tile adhesives or renderings for external walls. Two common additives to such mortars are cellulose ethers (CE) and redispersible polymer powders (RPP) [1,2]. The most important property of a CE is its water retention capability, which is especially needed when a fresh mortar is applied to an absorbing substrate. CE retains the water in the mortar for a sufficient time to allow proper cement hydration. Furthermore, CE are used to control the workability of fresh mortars, first by acting as a thickener and second by entraining air voids (about 25 % by volume). RPP are often added to improve mechanical properties. A key property of these mortars is their open time, defined as

* Corresponding author

the time during which tiles may be applied to the mortar surface and achieve adequate adhesion (i.e., the time during which the mortar surface remains "tacky" to the touch) [2]. Ultimately, this tackiness is lost due to the formation of a film at the top surface of the mortars. The film may be composed of both polymeric materials and (carbonated) hydration products. Jenni et al. [1] have used a variety of analytical techniques to study the polymer-mortar interactions in these materials. They observed, for example, that both the CE and the RPP are dissolved/redispersed in the pore solution and can form isolated films during drying. They also identified a fractionation process in which polymer components (and calcium hydroxide) were enriched at the top drying surface of the mortars. In this paper, the influence of drying on microstructural development of these mortars will be further studied utilizing x-ray absorption measurements.

Previously, x-ray absorption measurements have been applied successfully to studying drying of fresh cement-based materials [3-6] in the absence of thickeners. A summary of the observations made to date using this technique is as follows:

1) as opposed to drying from the exposed surface inward, thin (5 mm to 10 mm thick) specimens of cement paste and mortar, after initial set, dry out fairly uniformly throughout their thickness, with the largest pores throughout the thickness apparently emptying first [3, 4],
2) in bilayer composites, regardless of which layer is exposed to drying, water has always been observed to move from a coarser pore system to a finer one, whether the finer system is due to a finer cement at a constant water-to-cement ratio (*w/c*) or a lower *w/c* at a constant cement fineness [3, 4], and
3) in cement pastes containing a shrinkage-reducing admixture (SRA), the initial drying (first 8 h or so) does proceed from the exposed surface inward, followed by more uniform drying throughout the specimen; in this case, overall drying rates are reduced in the systems containing an SRA [5]. An example of the x-ray absorption results in this case is provided in Figure 1. As the specimen first dries out from the surface inward, the counts difference near the surface increases (a lower density is equivalent to more counts penetrating the specimen). For 13 h and beyond, a more uniform drying throughout the specimen thickness is observed.

Because a typical CE reduces the surface tension of the pore solution by an amount similar to the reduction provided by an SRA, it might be expected that the tile mortar adhesives containing CE will exhibit reduced drying rates and a drying front that proceeds from the exposed surface inward in comparison to control specimens prepared without CE. However, as will become clear in the remainder of this paper, the effects of the CE go far beyond a simple reduction in surface tension.

Materials and Experimental Procedures

Mortars were prepared in a round plastic container using a single blade rotary (kitchen) mixer. All dry ingredients (cement, sand, CE, and RPP and saturated lightweight fine aggregate (LWA) when present) were first homogenized in a sealed plastic bag. They were then placed in the mixing bowl and the appropriate mass of water added. Mixing then proceeded for 1 min, followed by a rest period of 3 min, then 30 s of final mixing. The mixture proportions and fresh

properties for the various mortars are provided in Tables 1 and 2. All mortars were proportioned on the basis of 300 g of dry ingredients (solids).

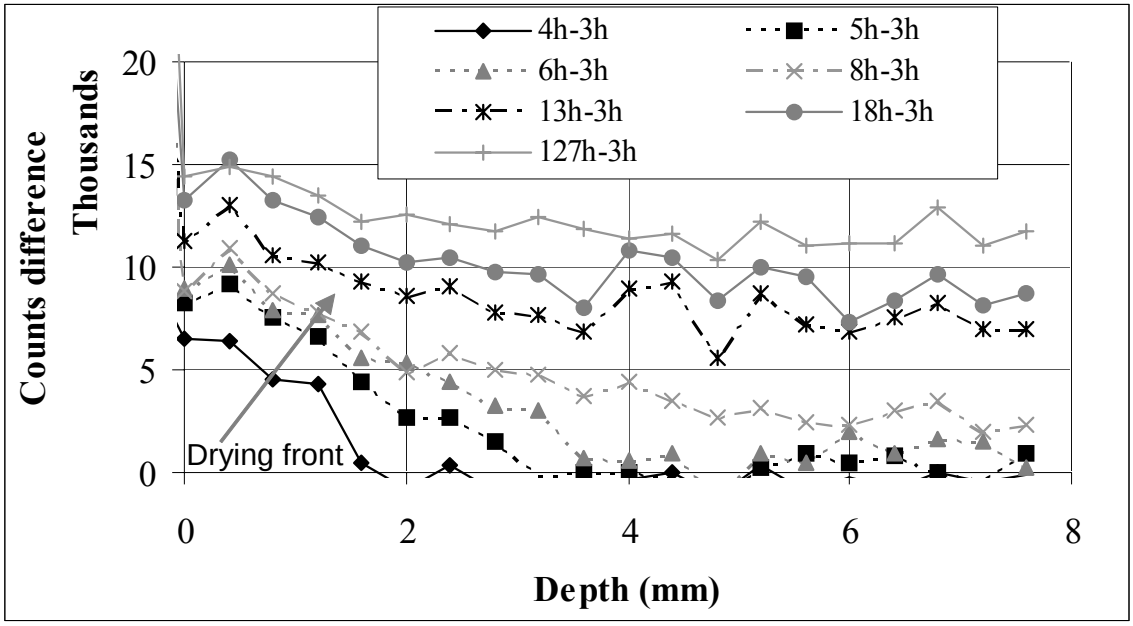

Figure 1. Example x-ray absorption results for a w/c=0.35 mortar containing an SRA (adapted from [5]). Counts difference indicates the difference between detected x-rays at the age indicated minus the value detected at 3 h.

Three different binder powders were utilized in the experiments. The first, which was used for the majority of the experiments, was a European CEM I 42.5 N cement. For one of the experiments, a coarse cement based on a previous sieving (air classification) of Cement and Concrete Reference Laboratory proficiency sample 135 [7] was employed. For the final experiment, a fine limestone [7] with a particle size distribution similar to that of the European cement was utilized. This experiment was conducted to remove any cement chemical reactions from the mortar and create a system where any changes in density would be purely due to physical and not chemical (hydration, carbonation, etc.) effects. The particle size distributions of the starting binder powders (cement, coarse cement, or limestone) were measured using a laser diffraction method. The measured differential distributions are provided in Figure 2.

Table 1. Detailed mixture proportions for mortar for experiments #1 and #6.

Material	Experiment 1 - Mass (g)	Experiment 6 - Mass (g)
Cement	107.4	107.4
Sand	191.7	101.0
Pre-wetted lightweight sand	None	62.5
Cellulose Ether	0.9	0.9
Water	66.0	66.0

Table 2. Mixture proportion details and fresh mortar properties for the various experiments.

Experiment	CE content (mass % of solids)	RPP content (mass % of solids)	Binder	Water (mass % of solids)	Pre-wetted LWA (mass % of total solids)	Fresh density with no air (kg/m^3)	Fresh air content (%)	Drying rate during 1st 2 h to 4 h ($kg/s)*10^8$	Open time (min)
1	0.3	None	Cement1	22	None	2.101	32.3	8.03	25
2	0.3	None	Cement1	26	None	2.03	25.8	12.28	50
3	0.3	3	Cement1	22	None	2.034	26.7	10.34	25
4	0.7	3	Cement1	22	None	2.026	20.3	7.90	15
5	0.3	3	Cement1	18	None	2.108	27.6	8.31	10
6	0.3	None	Cement1	24.3	23	1.941	26.1	11.30	65
7	0.3	None	Cement1	19.9	23	2.011	22.9	9.42	60
8	0.3	None	Coarse cement	22	None	2.101	34.2	9.83	5
9	0.7	None	Cement1	26	None	2.022	20.2	10.56	25
10	0.7	None	Cement1	22	None	2.092	26.3	7.97	10
11	0.3	None	Limestone	22	None	2.007	29.7	11.36	25

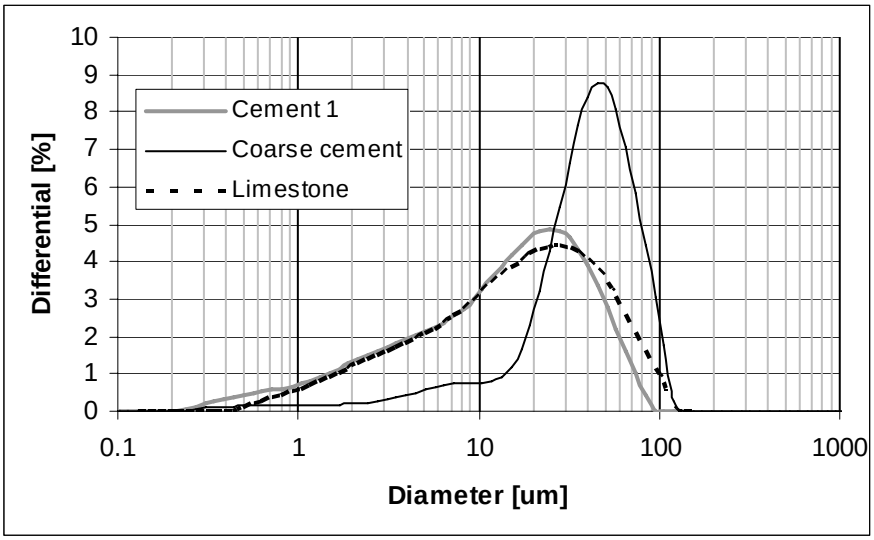

Figure 2. Measured particle size distributions for the various powders used in this study.

The prepared mortars were immediately placed into the sample holders for the x-ray absorption experiments and into small pre-weighed Petri dishes for the mass loss measurements. Initial masses of the filled Petri dishes, along with the volume of each dish, were used to estimate the air contents of the fresh mortars (Table 2). The average standard deviation in air content between duplicate specimens was 1.2 %. Mass loss measurements were generally performed over the course of 1 d and were used to estimate early-age drying rates for the different mortar mixtures (Table 2). Early-age drying rates were estimated based on the mass loss observed during the first 2 h to 4 h after casting and are included in Table 2. For reference purposes, the drying rate of a control specimen with no CE additive and 22 % water was (14 to 15) x 10^{-8} kg/s (fresh air content of only 2 % to 3 %). The average standard deviation in drying rates between duplicate specimens was 0.4 x 10^{-8} kg/s. The temperature and relative humidity inside the x-ray

absorption chamber and in the laboratory where the drying specimens were stored were monitored using USB-compatible data loggers throughout the course of the experiment. The average temperature and RH in the laboratory were 21.6 °C and 29.7 %, respectively. The corresponding values in the x-ray chamber were 25.2 °C and 25.5 %. Based on these values, the differences between the two environments were not considered to be significant when comparing the mass loss and x-ray absorption results.

The sample holder for the x-ray absorption experiments is shown in Figure 3. Generally, the mortars were applied in two layers and a small round glass rod was used to tamp the individual layers. Smoothing and leveling of the top surface was then completed using a small metal spatula. The same mortar was loaded into both sides of the specimen holder and one half was sealed with two layers of tape to provide a sealed reference sample. The prepared specimen holder was then placed into the x-ray absorption chamber and monitored over the course of time. The details of the x-ray absorption equipment have been provided elsewhere [3-6]. For these experiments, a voltage of 40 keV and a current of 150 μA were used, along with a 30 s exposure. An x-ray camera detector provides a 256 pixel by 252 pixel 16-bit image for each exposure. Each pixel is approximately 0.1 mm x 0.1 mm in size. Previously, the relative standard uncertainty in (detected) counts has been determined to be on the order of 0.4 % [4]. The collected images were analyzed using a combination of C programs and the Dataplot graphical and statistical analysis software package [8]. The sealed reference sample portion of the obtained images was used to normalize the results for variation in the intensity of the x-ray signal, etc. from one exposure time to the next. The normalized x-ray results were then plotted as average counts vs. depth and as the difference in this quantity between the initial evaluation time and each subsequent time.

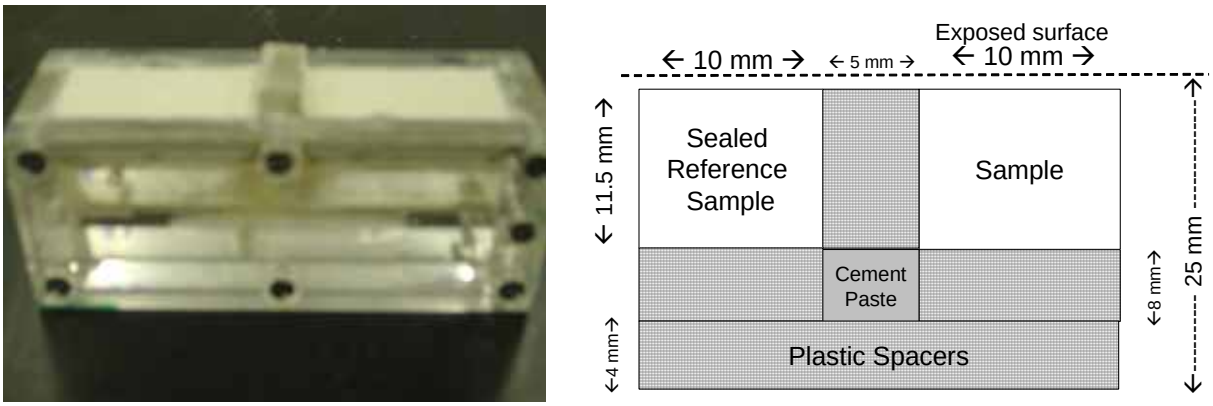

Figure 3. Photograph of sample holder and schematic of area viewed by x-ray camera detector during the x-ray absorption experiments.

In separate experiments, the viscosities of solutions with various additions of cellulose ether (CE) were measured at 24 °C using a Hoeppler falling ball viscometer (uncertainty of less than 1 %) and the open times of the various mortars were measured according to European Standard EN 1347 (Determination of the wetting capability) [9]. Using this test method, a layer of a tile adhesive is combed onto a concrete slab using a notched trowel. Glass plates (100 mm × 100 mm × 6 mm) are embedded in the fresh mortar after 5 min, 10 min, 15 min, etc., from which the ability of the combed material to wet the glass plates is assessed. Only samples with a wetted

area > 50 % pass the test. The viscosity results are provided in Figure 4. To estimate the viscosity for various concentrations of CE that were not measured directly, the measured data was fitted to a cubic polynomial, as shown in Figure 4. The open time results are included in Table 2 and will be discussed in the Results section to follow.

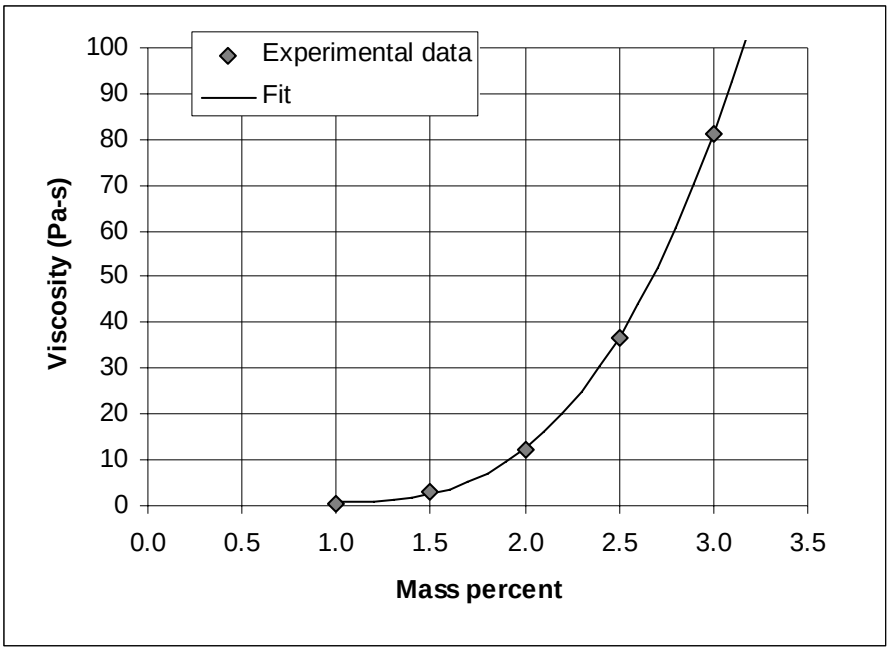

Figure 4. Measured viscosities for cellulose ether (CE) solutions. Fitted equation is of the form: Viscosity = $10.88CE - 17.62CE^2 + 7.66CE^3$, with CE in mass percent.

Results and Discussion

The first experiment was conducted on a mortar mixture containing only cellulose ether at a typical addition rate and produced a mortar with an open time of 25 min. The x-ray absorption results for this experiment are presented in Figure 5, both in terms of the average counts as a function of depth from the exposed (top) surface and in terms of the counts difference between the initial measurement (at 15 min) and each subsequent measurement. A drying front penetrating into the specimen, as indicated by an increase in the counts for x-rays going through the specimen near the exposed surface, is clearly observed in the counts difference plot, as would be expected from previous observations on cement pastes containing an SRA (see Figure 1) [5]. However, the results in Figure 5 also differ from those in Figure 1 in at least two ways. Upon careful examination of the plots, there is an indication of a densification front penetrating into the specimen in front of the drying front. This would be indicated by the counts difference curve for a specific time (135-15 for example) falling below that of the immediately preceding time (110-15) at distances just beyond the end of the drying front. When the counts decrease from one exposure time to the next, this indicates that fewer x-rays are going through the specimen, in agreement with an increase in its local density. While this densification appears rather small in Figure 5, it must be kept in mind that it was expected for the counts difference curves to increase with time as the drying front penetrates into the specimen, so that the observed (small) decrease is actually larger when this expected increase is properly considered. In addition, the large change in the counts difference plot at a depth of about 7 mm from the exposed top surface of the

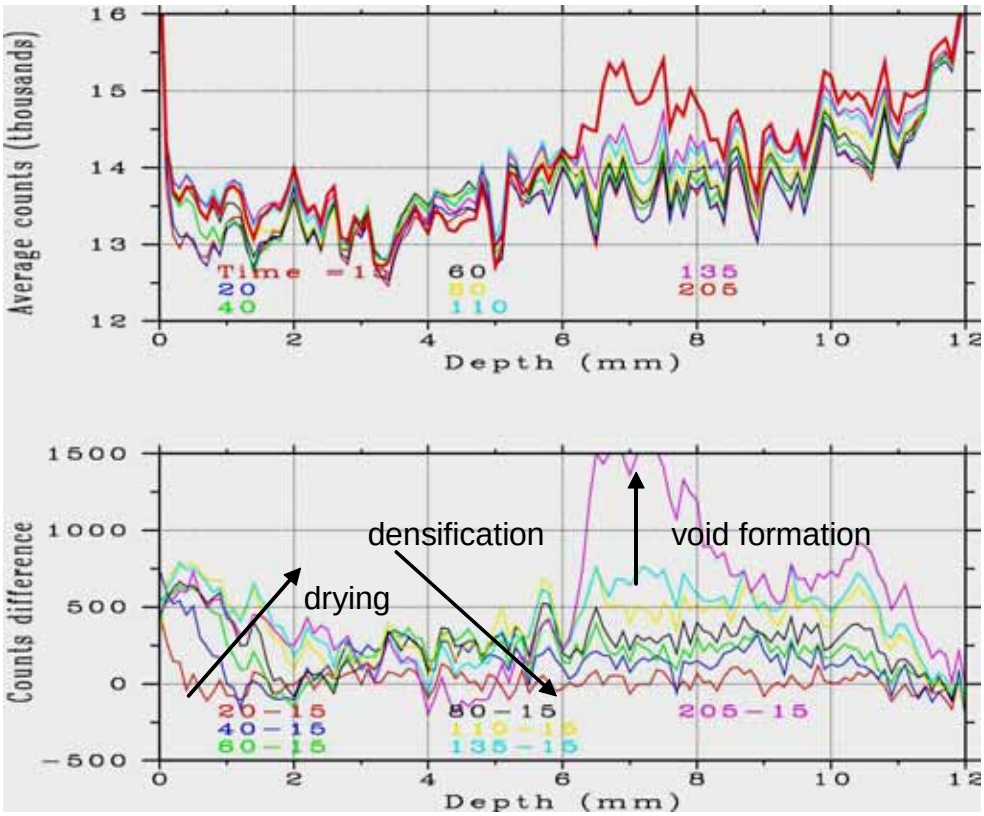

Figure 5. X-ray absorption results for experiment #1. Times in legend are in minutes from time of mixing.

specimen between 135 min and 205 min had not been observed in any of the previous x-ray absorption experiments [3-6]. These results suggest that additional phenomena beyond the simple removal of water are occurring in these materials.

Next, the water content of the mortar was increased from 22 % to 26 % for experiment #2, which resulted in a substantial increase in the open time (Table 2). The x-ray results for this experiment are provided in Figure 6. Now, while the drying front is not so clearly visible, perhaps due to the increased drying rate and dilution of the cellulose ether, the densification front from 15 min to 40 min and the extreme decrease in density after 2.5 h at about 7 mm depth are more significant. (It should be noted that the scale range for the counts difference plot in Figure 6 is four times that in Figure 5.) After much discussion, it was hypothesized that the most likely explanation for the surprising x-ray results is that the high viscosity fluid in the mortar specimens is carrying small particles along with it throughout the drying process. This could explain the observation that the densification front occurs immediately adjacent to the drying front, as the smaller particles would be sequentially deposited at the location of the penetrating evaporation front. The large changes in local density noted at a depth of about 7 mm in Figures 5 and 6 could then be due to the replacement of a large volume fraction of small particles and pore fluid by air. In support of this, when several of the dried mortar specimens were observed at the end of their exposures, large voids several mm in size were noted near the middle (thickness) of the specimens (see Figure 7 for an example of this). It is unlikely that these voids were present during the initial specimen preparation and furthermore, no such voids were observed in the specimens cured under sealed (minimal if any drying) conditions (Figure 7). To

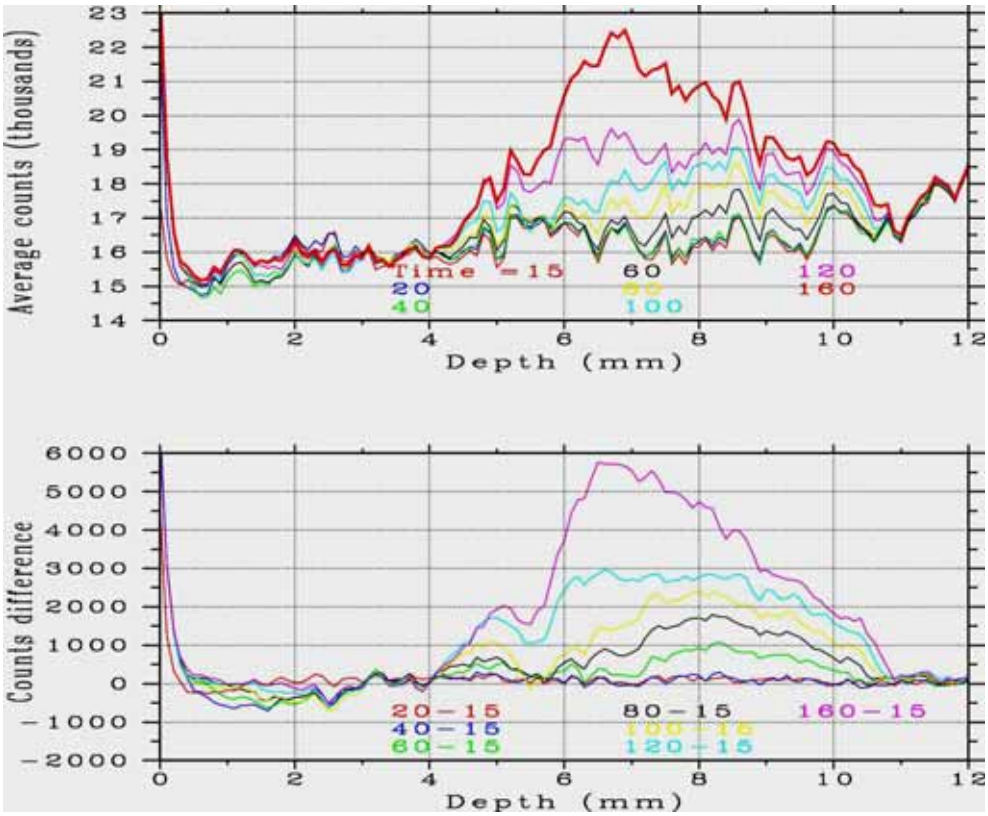

Figure 6. X-ray absorption results for experiment #2, with an increased water content.

investigate this possibility further, an analysis based on applying Stokes equation to the various experiments was conducted.

Stokes equation conventionally describes the settling velocity of a particle in a fluid. This same equation can be utilized to determine the maximum diameter for a particle that will be carried along with a fluid moving at a given rate during the drying of the mortar specimens. Instead of the particles settling through the fluid, the fluid is moving at a fixed velocity and the particles may remain stationary or be carried upward along with the fluid, depending on their diameter and density, as well as the density and viscosity of the fluid itself. The magnitude of the equilibrium velocity of a cement particle falling through a viscous fluid is estimated using the Stokes formula for the viscous drag on a sphere [10]:

$$v = \frac{d_s^2}{18\eta_f}(\rho_s - \rho_f)g \tag{1}$$

where v is the speed of the particle in the fluid (m/s), d_s is the particle diameter (m); η_f is the fluid dynamic viscosity (Pa·s); ρ_s and ρ_f are the densities of the solid particle and fluid (kg/m^3); and g is the gravitational acceleration (9.81 m/s^2). This speed represents the minimum upward velocity required to "lift" a spherical particle of diameter d_s. To apply this equation to the current problem, by assuming a system of cylindrical pores extending through the thin mortar specimen, the velocity (drying rate) can be estimated from the mass loss measurements as:

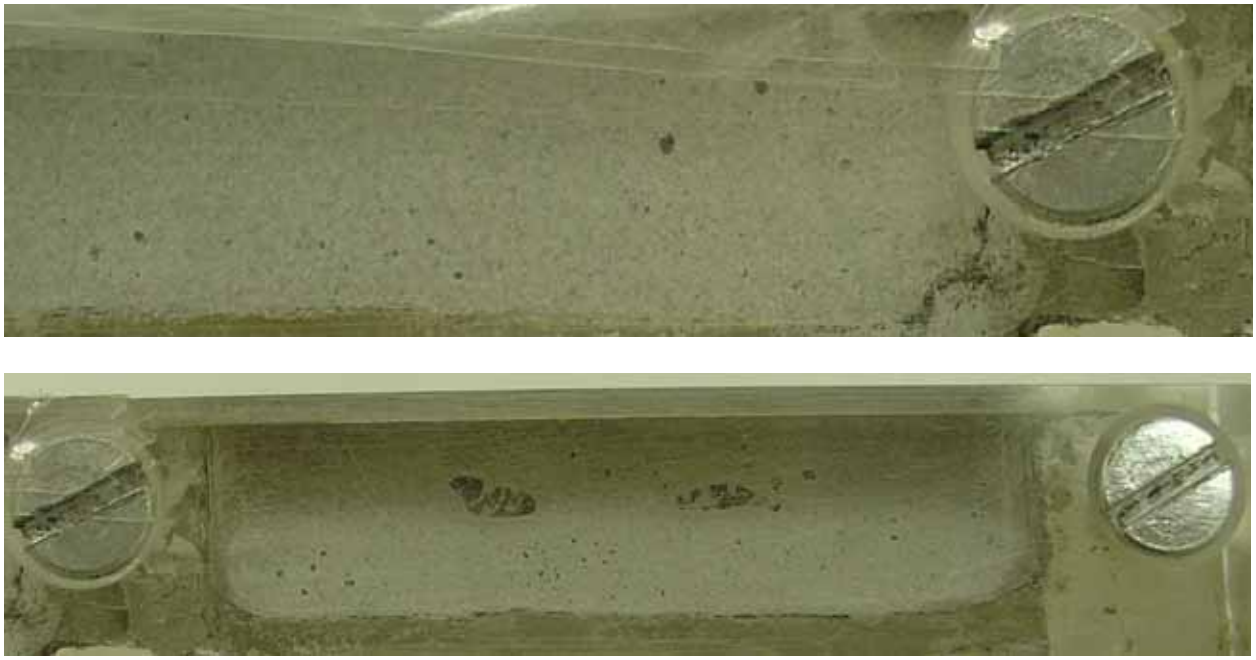

Figure 7. Photographs of side edges of sealed (top) and exposed to drying at its top surface (bottom) tile adhesive specimens at the end of experiment #9. Two "eye-shaped" voids (dark) several mm in size can be seen in the middle of the specimen exposed to the drying environment.

$$v = \frac{\frac{dm}{dt}}{\rho_w A \phi (1-\alpha)} \tag{2}$$

where v is the estimated velocity (drying rate); dm/dt is the change in mass per unit time (kg/s); ρ_w is the density of the evaporating water; A is the area of the Petri dish drying sample holder (0.00178 m^2); ϕ is the initial volume fraction of water in the fresh mortar mixture (equivalent to the capillary porosity with no air); and α is the air content (fraction) of the fresh mortar mixture as provided in Table 2. An approximation to the maximum particle diameter that can be transported by the moving pore solution is estimated from equating Eqn. 1 and Eqn. 2 and solving for the diameter d_s. This approximation assumes a constant fluid viscosity during drying, does not account for the effect of pore volume tortuosity on instantaneous velocity, and assumes that the pore diameter is many times larger than the maximum particle diameter. While this latter assumption is certainly not valid for the mortars in this study, the analysis will provide an estimate of the particles sizes whose movement during drying could be influenced by the high solution viscosities.

Based on the drying rates given in Table 2, the estimated maximum particle diameters for particles moving with the drying fluid are provided in Table 3. Surprisingly, the particle diameters are on the order of tens of micrometers, up to slightly more than 100 μm in a few cases. As mentioned above, these values are surely overestimates, but particles one to five micrometers in diameter, for instance, are likely to be mobile during the early-age drying of these mortars. It is interesting to note that for a conventional pore fluid with a viscosity near 0.001 Pa·s, the maximum particle diameter would be less than 0.5 μm. In such a mortar, while few if any

cement particles would migrate to the top surface during drying, newly formed "microcrystals" of calcium hydroxide could well do so, contributing to the layer of calcium hydroxide "crystals" often observed at the top surface of cement-based materials (usually attributed to only ionic species being carried to the top and precipitating there).

Table 3. Estimated Maximum Particle Diameter for Movement During Each Experiment

Experiment	Estimated (Fig. 3) Fluid Viscosity (Pa·s)	Solid Density (kg/m^3)	Drying velocity during 1st 2 to 4 h ($m/s*10^8$)	Maximum Particle Diameter (μm)
1	1.5	3200	17.6	15
2	0.87	3200	20.3	12
3	2.2	3200	20.6	16
4	103.1	3200	13.9	109
5	4.68	3200	19.1	27
6	1.5	3200	22.8	17
7	4.68	3200	19.7	28
8	1.5	3200	22.2	17
9	51.2	3200	16.3	83
10	103.1	3200	16.1	118
11	1.5	2710	21.9	19

In experiment #3, RPP was added to the mortar utilized in experiment #1, resulting in an equivalent open time to that achieved in the first experiment. The x-ray absorption results for this experiment are provided in Figure 8. While the measured drying rate (Table 2) is slightly higher for the system with the RPP, its presence appears to stabilize the mortar such that only a minor densification and a slight increase in local density after 3 h at a depth of about 6 mm are observed. The RPP may form a semi-rigid network throughout the microstructure that may act as a filter (net) to prevent large scale (mm) movement of the smaller particles along with the high viscosity fluid.

As shown by the results in Figure 9 and Table 3 for experiment #4, a further increase in the CE content results in a large increase in the fluid viscosity and a reappearance of both the densification front and the large decrease in local density at a depth of about 6 mm, despite a significant decrease in the drying rate (Table 2). According to equations (1) and (2), particles as large as 100 μm in diameter could be moving with the fluid during drying in this experiment, although, as mentioned earlier, it seems unlikely that pore channels of sufficient diameter for such movement would exist in the three-dimensional microstructure. The open time for this experiment exhibited a decrease to 15 min.

In experiment #5, the water content of mixture #3 was reduced from 22 % to 18 %, increasing the pore fluid viscosity by a factor of about 2.5, but decreasing the "diameters" of the pore channels between particles. As shown by the x-ray results in Figure 10, this resulted in a mortar with equal stability to that of mortar #3 (Figure 8), exhibiting only minor drying and densification fronts and some evidence of a local density decrease after 2.5 h at a depth of 10 mm. However, the measured open time for this "stable" mortar was further reduced to only 10 min.

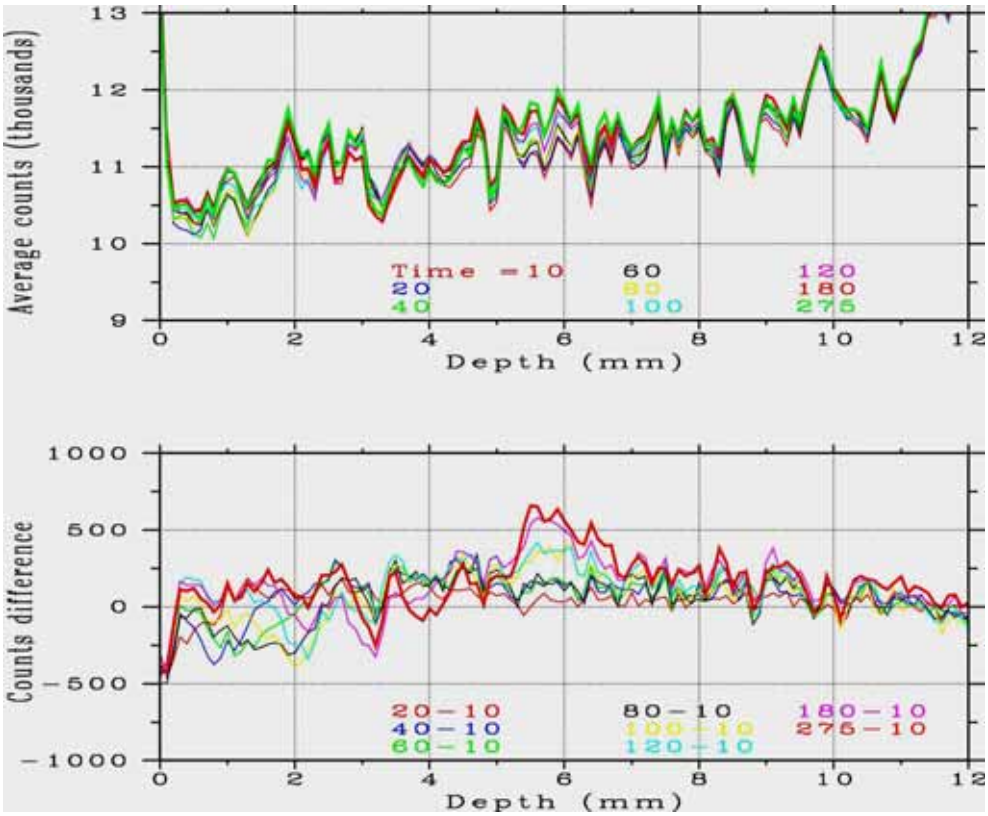

Figure 8. X-ray absorption results for experiment #3, with an addition of RPP to the mortar.

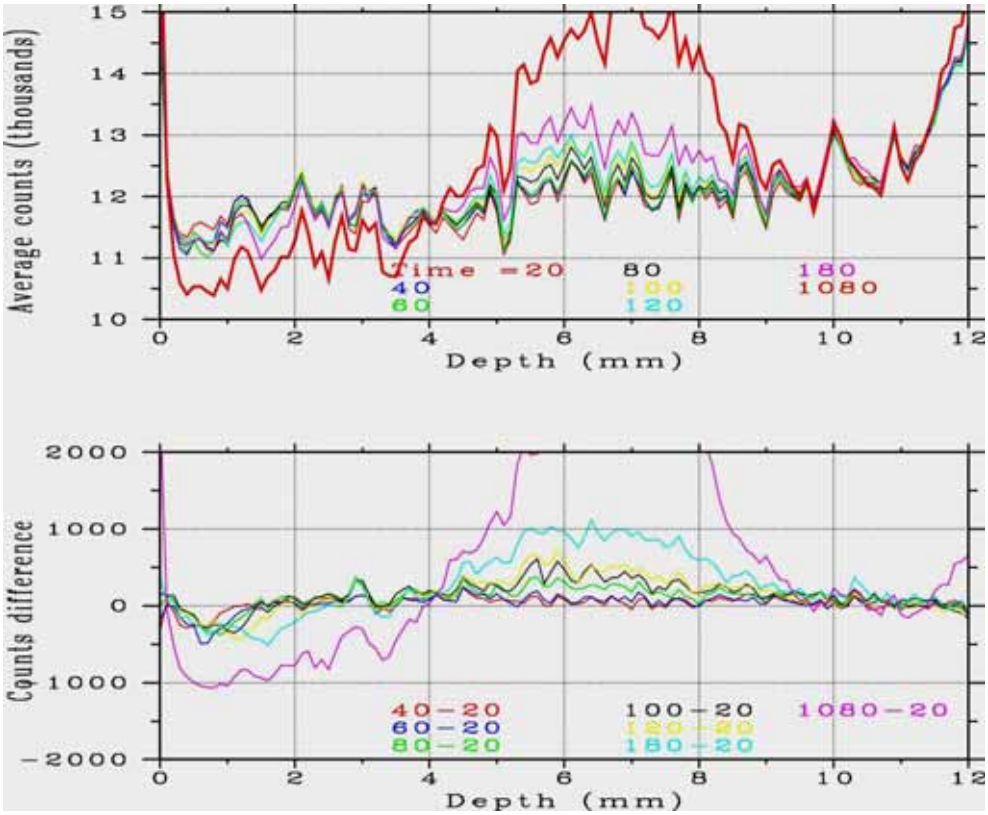

Figure 9. X-ray absorption results for experiment #4, with an increased CE content.

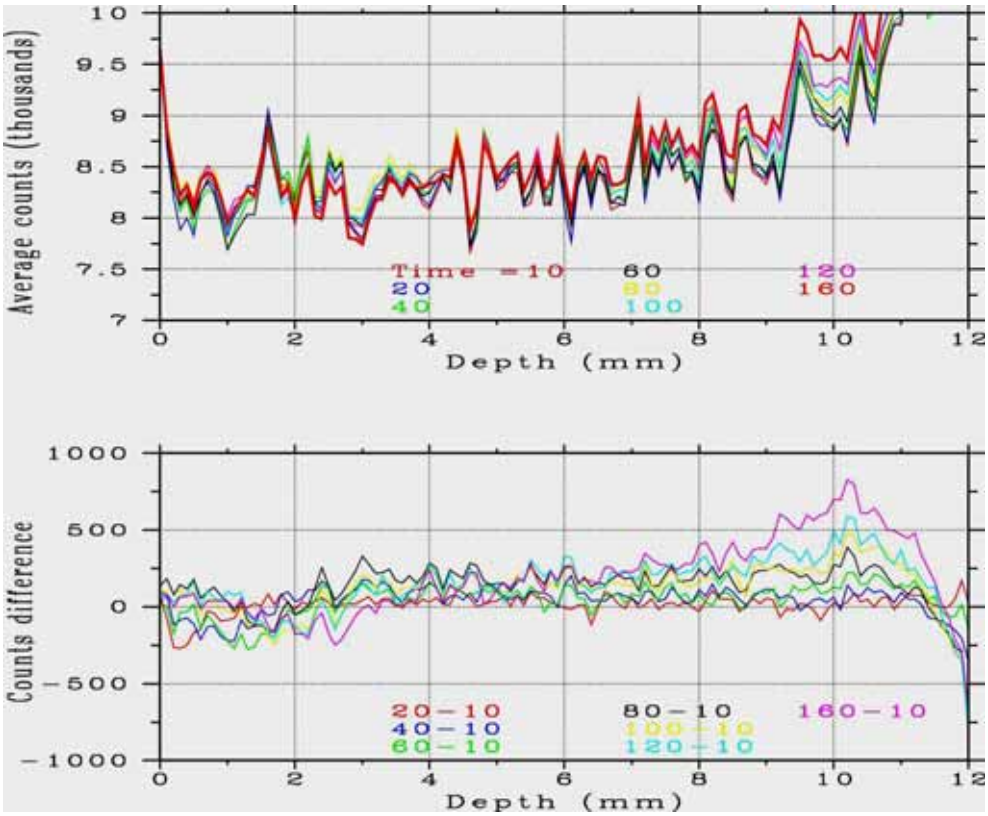

Figure 10. X-ray absorption results for experiment #5, with a reduced water content.

Beginning with experiment #6, a few methods for mitigating these negative effects (instabilities) were investigated. Experiments #6 and #7 considered the incorporation of a pre-wetted LWA (an expanded shale) with an absorption of 23.8 % [11] into the mortar mixtures to provide an extra reservoir of low viscosity curing water. Experiment #6 increased the open time to 65 min, but resulted in an unstable mortar with bleeding and some settlement, followed by the creation of a large densification front penetrating 6 mm into the mortar from the exposed surface. Due to this unacceptable performance, this experiment was terminated after only 60 min of exposure. In experiment #7, the same amount of pre-wetted LWA was added to a system with a mixing water content of 20 %, for a total water content of 24.3 %. As shown in Figure 11, this system exhibited only a small drying/densification front with very uniform drying at later ages (1160 min). The measured open time for this mortar, 60 min, was over double that of experiment #1. If some of the pore fluid passes through the LWA during drying, the porous LWA may serve to filter out some of the smaller particles that would otherwise be carried along with the drying fluid to the evaporative surface of the specimen, restricting particle movement to be a localized as opposed to a longer distance (5 mm) phenomenon.

In experiment #8, a different approach was taken to mitigating the negative impacts on microstructure development during drying by utilizing a coarse cement with only a small fraction of particles smaller than 20 μm in diameter (Figure 2). As shown in Figure 12, this resulted in a stable mortar whose drying behavior was quite similar to that observed previously for cement-based materials containing an SRA (Figure 1) [5], and basically what was expected to be observed when these experiments were initiated. Initially, there is a clearly observable drying

front, followed by uniform drying at later ages (960 min). However, the measured open time for this mortar was only 5 min.

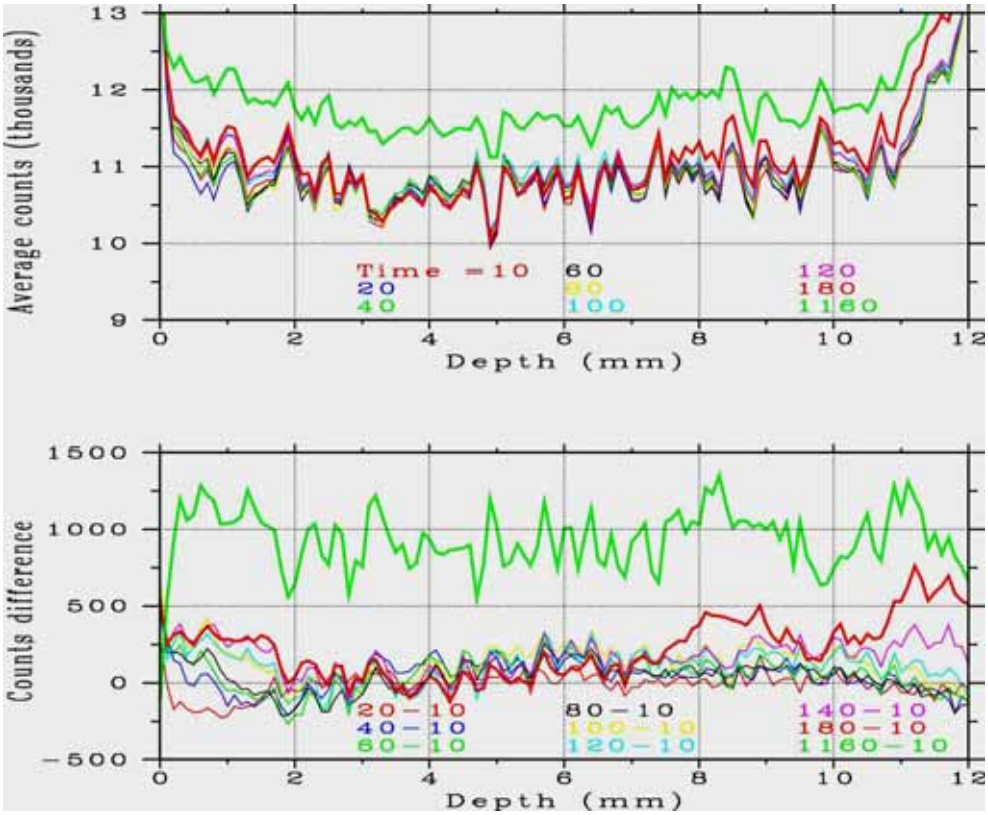

Figure 11. X-ray absorption results for experiment #7, with the addition of pre-wetted LWA.

Two additional experiments were conducted in systems with a high dosage of CE and water contents of 26 % (experiment #9) and 22 % (experiment #10). The x-ray results are provided in Figures 13 and 14, respectively. Ultimately, neither of these mortars exhibits a high degree of stability, although both resulted in slightly reduced drying rates relative to their low CE dosage counterparts in experiments #2 and #1, respectively (Table 2). Both figures exhibit the now characteristic densification fronts and the formation of local regions of low density at later ages. In experiment #9, there is some evidence of bleeding and local settlement at the top surface for the mortar (Figure 13), as evidenced by a shift to the right for the sharp increase in counts difference at the very top surface of the specimen. In terms of ultimate instability, the results are more pronounced in the system with a lower water content (Figure 14) where significant decreases in density (increases in counts difference) are observed after 200 min at depths of both 4 mm and between 8 mm and 10 mm.

In a final experiment, the European cement was replaced with an inert limestone powder with a similar particle size distribution (Figure 2). The purpose of this experiment was to verify that the particle movement and accompanying densification is mainly a physical phenomenon and has little to do with cement chemistry, carbonation, etc. As shown in Figure 15, significant densification and instability (void formation) were present in this mortar, further confirming the hypothesis that the movement of small particles along with the high viscosity pore fluid during drying is largely responsible for the densification observed at the top surface of the mortar.

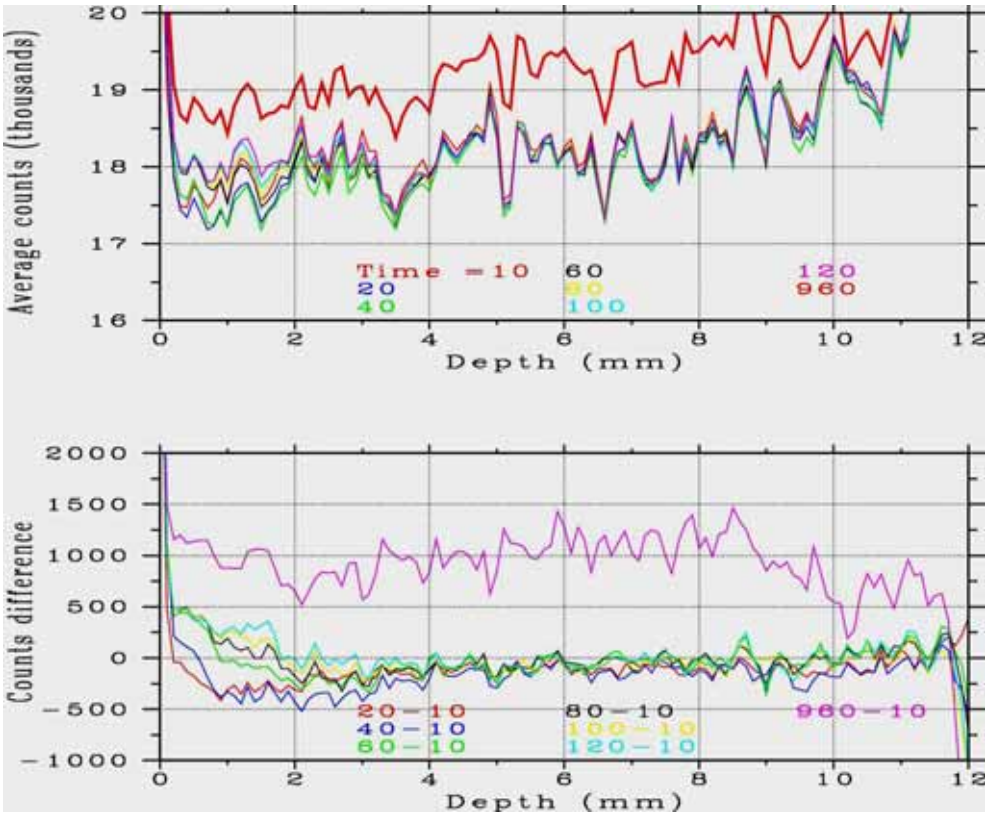

Figure 12. X-ray absorption results for experiment #8, using a coarse cement.

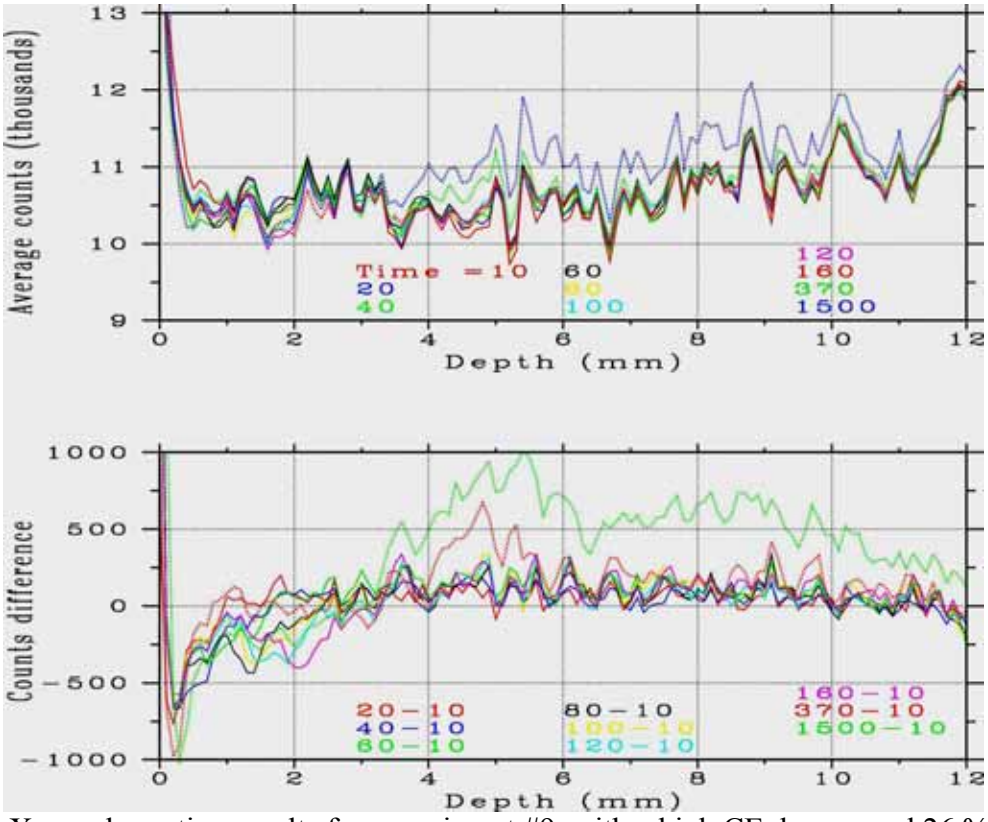

Figure 13. X-ray absorption results for experiment #9, with a high CE dosage and 26 % water.

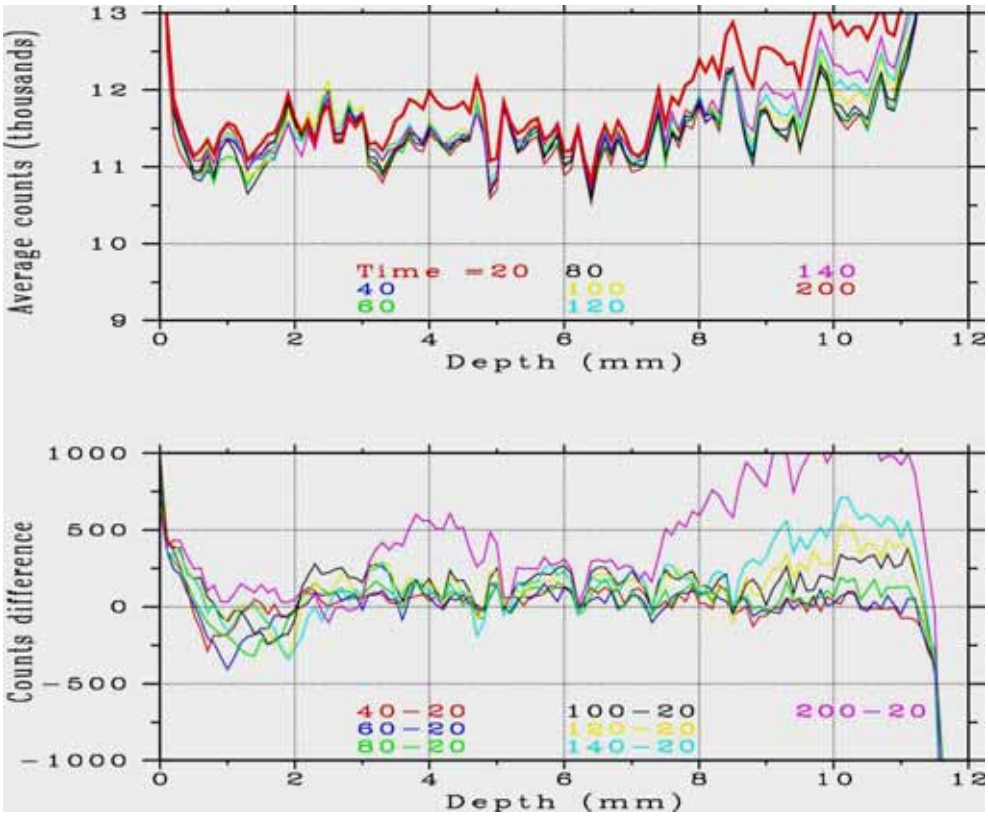

Figure 14. X-ray absorption results for experiment #10, with a high CE dosage and 22 % water.

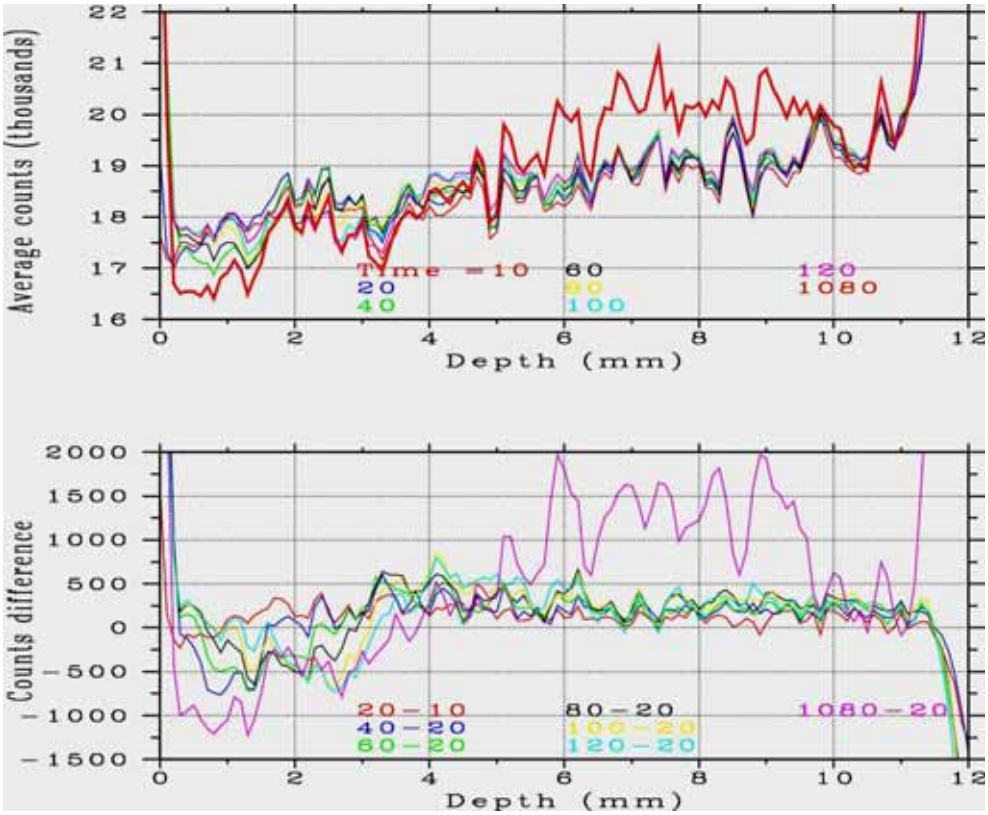

Figure 15. X-ray absorption results for experiment #11, using a limestone powder.

Since the limestone mortar is inert and contains no cement to react with the water, it doesn't set even after a day of drying. Thus, as a final check on the hypothesis, the completely dried specimen was carefully sectioned into three layers representing the top, middle, and bottom of the sample. The powder from the sectioned layers was placed in crucibles that were placed in a furnace at 400 °C to burn off the CE and then subjected to particle size distribution analysis. The obtained cumulative particle size distributions are provided in Figure 16. From the figure, the volume fraction of smallest particles is clearly enhanced in the top and middle layers of the mortar in agreement with the x-ray profiles in Figure 15 and the basic hypothesis concerning particle movement.

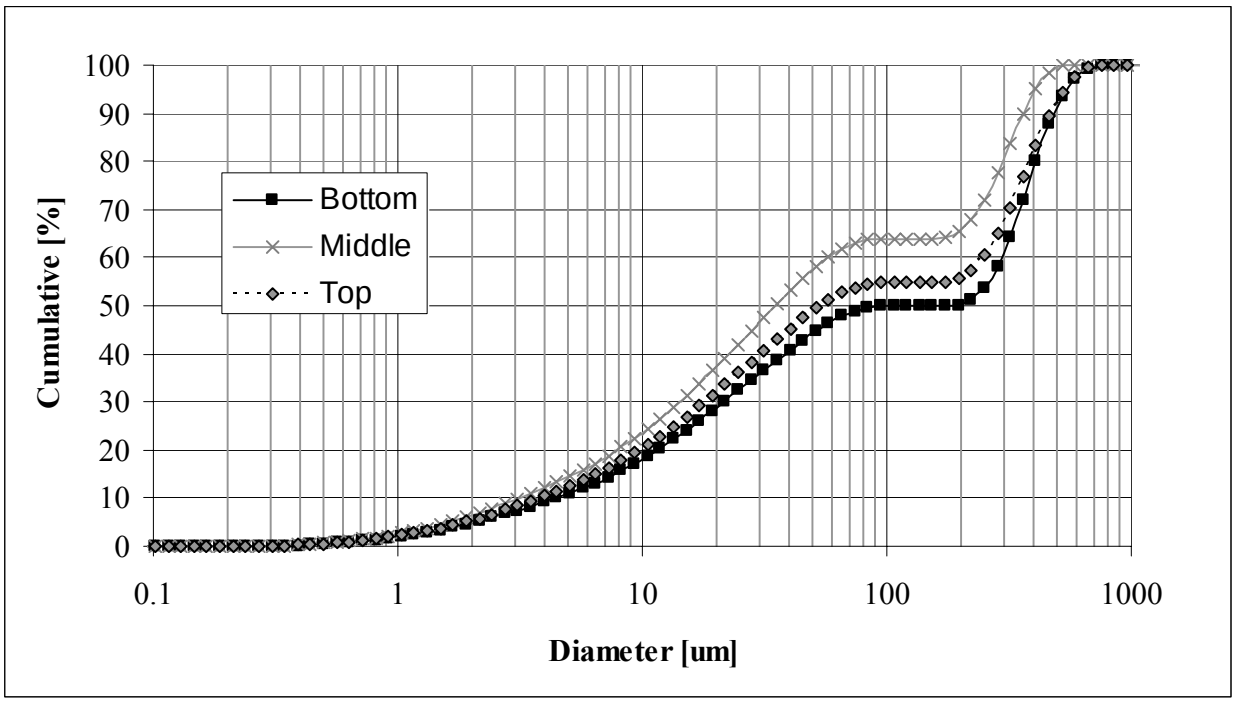

Figure 16. Cumulative particle size distributions for top, middle, and bottom portions of the limestone mortar specimen at the end of experiment #11.

While the results of these experiments and the verification of the hypothesis that small particles are mobile during the drying process in these high viscosity systems is of basic scientific interest, it is worthwhile to return to the performance characteristics of the tile adhesives and discuss the impact of these observations. The formation of these large void regions could be partially responsible for the unusually low later age tensile strengths sometimes exhibited by these materials, especially if the voids are formed at or near the interface between mortar and substrate. Voids of several mm in size would surely result in substantial strength reductions. In terms of open time, the densification of the top surface by the smaller particles in the system likely contributes to a reduction in the open time by further decreasing the "tackiness" of the top surface. Furthermore, their movement results in a concentration of the most reactive cement particles at the top surface of the mortar where their more rapid hydration could further contribute to a reduction in open time both by reducing free water content and by stiffening the paste. Thus, from a practical standpoint, it would seem to be beneficial to formulate a mortar where this particle movement is minimized and these large decreases in local density do not

occur. The addition of RPP, the utilization of a coarser cement, and the incorporation of pre-wetted lightweight aggregates all appear to offer the potential to achieve such a formulation. However, in viewing the open time results in Table 2, the open time performance of the three mortars with the RPP additions (experiments 3-5) are no better than those of the base system investigated in experiment #1. While it is conjectured that the RPP stabilizes the particle movement due to the formation of a polymer network, this same network may substantially contribute to film formation at the exposed (drying) surface, preventing a longer open time. On the other hand, the two systems with the pre-wetted LWA additions (experiments 6 and 7) provided open times that were more than double that of the base system. While experiment #6 produced a highly unstable system in terms of bleeding and densification at the top surface, experiment #7 produced a stable mortar with a greatly increased open time that may be worthy of further investigation. The coarse cement system (experiment 8) also produced a stable mortar but with an open time of only 5 min, and its lower reactivity and slower strength development must also be considered. Thus, while extensive laboratory and field testing will be needed to further evaluate the feasibility and robustness of each of these approaches, the approach based on pre-wetted lightweight fine aggregates appears to be the most promising at this point in time.

Conclusions

X-ray absorption measurements performed during the drying of typical mortar tile adhesives have suggested a new mechanism contributing to film formation at the exposed (drying) surface, namely the mobility of small cement particles carried along by the drying fluid, due to the extremely high viscosities of the pore fluids containing cellulose ethers. This particle movement is exemplified by the development of a densification front occurring immediately adjacent to the penetrating drying front. An additional effect of the drying/particle movement can be the formation of internal voids (and regions of low density) several mm in size within the mortar. Such voids could significantly reduce the final strength properties of these materials. Possible mitigation strategies to minimize the particle movement during drying in high viscosity mortars include utilizing a coarser cement, including a redispersible polymer powder, and incorporating internal curing via the addition of pre-wetted lightweight aggregates. Further evaluation of these technologies will be required to determine their usefulness in practical applications under field conditions.

Acknowledgements

C.J. Haecker would like to thank the staff of the Inorganic Materials Group at the National Institute of Standards and Technology (NIST) for hosting a visit during which these experiments were completed. The authors would also to thank Northeast Solite Corporation for providing the lightweight aggregates used in this study and Duane Emmett of Bostik, Inc. for useful discussions.

References

1) Jenni, A., Holzer, L., Zurbriggen, R., and Herwegh, M., “Influence of Polymers on Microstructure and Adhesive Strength of Cementitious Tile Adhesive Mortars,” Cement and Concrete Research 2005; 35: 35-50.

2) Oberste-Padtberg, R., and Sieksmeier, J., “Factors Influencing the Open Time of Building Mortars,” Drymix Mortar Yearbook 2007: 44-49.
3) Bentz, D.P., and Hansen, K.K., “Preliminary Observations of Water Movement in Cement Pastes During Curing Using X-ray Absorption,” Cement and Concrete Research 2000; 30: 1157-1168.
4) Bentz, D.P., Hansen, K.K., Madsen, H.D., Vallee, F.A., and Griesel, E.J., “Drying/Hydration in Cement Pastes During Curing,” Materials and Structures 2001; 34: 557-565.
5) Bentz, D.P., Geiker, M.R., and Hansen, K.K., “Shrinkage-Reducing Admixtures and Early Age Desiccation in Cement Pastes and Mortars,” Cement and Concrete Research 2001; 31: 1075-1085.
6) Bentz, D.P., “Influence of Curing Conditions on Water Loss and Hydration in Cement Pastes with and without Fly Ash Substitution,” NISTIR **6886**, U.S. Department of Commerce, July 2002.
7) Bentz, D.P., “Replacement of “Coarse” Cement Particles by Inert Fillers in Low w/c Ratio Concretes II: Experimental Validation,” Cement and Concrete Research 2005; 35: 185-188.
8) http://www.itl.nist.gov/div898/software/dataplot/, access verified May 2007.
9) EN 1347, "Adhesives for tiles - Determination of wetting capability,” Comité Européen de Normalisation Technical Committee 67, 1999.
10) Landau, L.D. and Lifshitz, E.M., “Fluid Mechanics,” (Second Edition) Pergamon Press, New York, 1987.
11) Bentz, D.P., “Internal Curing of High-Performance Blended Cement Mortars: Autogenous Deformation and Compressive Strength Development,” ACI Materials Journal, July-Aug. 2007; 104 (4):408-414.